Theoretical Band and Confinement Interpretation of 1D Electrons: Impact on Plasmons and Exchange-Correlation Functionals

Akariti Sharma (✉ akariti@prl.res.in)

PRL: Physical Research Laboratory   https://orcid.org/0000-0002-9675-8654

Research Article

Theoretical Band and Confinement Interpretation of 1D Electrons: Impact on Plasmons and Exchange-Correlation Functionals

Akariti Sharma

Abstract Theoretical band and confinement interpretation of electron gas in lowest energy sub-band of quasi-1D metallic wire have been done. Counter effects have been investigated on electrostatic oscillations (plasmons) determined by the electron density response function. Carrier correlations are treated by incorporating the local exchange-correlation (XC) effects within mean-field approximation. Results obtained are in quantitative agreement with experiments data of Nagao *et al.* (2006 Phys. Rev. Lett. 97 116802). Variation in both degeneracy and confinement potential cause a clear energy-shift in the electrostatic oscillations accomplished by asymmetry in band effective mass. Resultant mass-asymmetry is attributed to the greater strength of XC-effects. These contributions turns out to be quite logical in describing the splitting of 1D-bands over ad-hoc spin-orbital splitting idea of Nagao *et al.* Calculated XC-functionals agreed well with the lattice regularized diffusion Monte Carlo (LRDMC) simulation data (2006 Phys. Rev. B 74, 245427, 2009 J. Phys. A: Math. Theor. 42 214021). Competition among XC-functionals and kinetic energy tendencies decides a criterion by satisfying which a metallic quasi-1D wire may undergo an instability at certain critical temperature (T_c).

Akariti Sharma
Theoretical Division, Physical Research Laboratory Ahmedabad, Gujarat, India
Tel.: +91 7009413945
E-mail: akaritisharma@gmail.com

1 Introduction

In Physics, Plasmonics relates to the electrostatic oscillations in low-dimensional (LD) metallic systems like nanotubes, nanowires and nanorodes [1–3] which having great technological importance. In particular, the study of plasmons in quasi-1D electrons systems has generated considerable theoretical [4–9] as well as experimental [10–13] interest. The technological progress at nano-scale allows researchers to produce a new class of plasmonic systems called quasi-1D wires having narrow (nm or Å) 1D channels. Example includes, confined 1D electron densities at the interface of $AlGaAs$–$GaAs$ hetero-structures [10, 14] and array of Au-induced 1D chains on $Si(111)$ surfaces [11, 12]. Schematically, the 2D electron gas (2DEG) beneath the gates is repelled
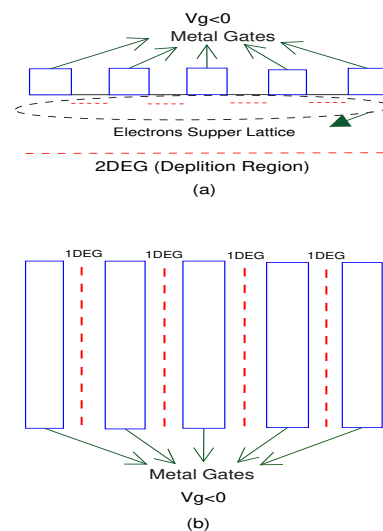
Fig. 1 A set of gates used to form 1D electrons super lattice, lateral view [in panel (a)] and top view [in panel (b)].

by negative voltage on the gates and construct a supper lattice of 1D electrons gas (1DEG) shown in figure 1. So far, Au chains grown on $Si(557)$–Au surface have attracted much attention due to presence of many intriguing phenomenon such as spin-charge separation [15], Peierls instability, metal-to-insulation transition (MIT) [20], spin-orbital coupling (SOC)[16] etc. due to increased XC-effects. The existence of enhanced XC-effects is frequently associated with non-local dynamics of carriers [7]. However, the existence of non-local dynamics is not a necessary condition for the increased XC-effects. Interestingly, the band and confinement interpretation can also enhance the XC-effects in LD systems [19].

Angle-resolved photoemission (ARP) showed that $Si(557)$–Au surface possess two proximal electron bands and the Fermi-level crossings of these two bands are separated [15]. As a result of which $Si(557) - Au$ surface is metallic despite of having an even electron count. According to ab-$initio$ studies [16], 1D band associated with the $Si(557) - Au$ surface develops appreciable splitting of ($\approx 0.3eV$) as consequence of spin-orbit (SO) coupling, and both the bands are metallic. On the other hand, Ahn et $al.$ [17] have found that only one splitted-band is metallic at $T = 300K$ and other is insulating at finite-T close to absolute zero. They also claimed that at least one of the two splitted-bands should be associated with the step-edge atoms. A step head, Alt et $al.$ [18] have found that these two bands associates with two nearly degenerate atomic chains, or a chain of step atoms with two broken bonds. Further, Nagao et $al.$ [11, 12] have measured the electrostatic oscillations in the Au chain on the $Si(557)$–Au surface by using electron-energy-loss spectroscopy (EELS). They noted that Au chain/wire is found to exhibit 1D-metallic characteristics in one of the SO-splitted band. In spite of these efforts, the surface electronic structure of $Si(557)$–Au system is not completely understood up to now. Also, the exact nature of 1D-bands and cause of splitting is unclear.

Motivated by these studies, the cause, nature and association of splitted 1D-bands are discussed here on the basis of XC-functional in a deliberate manner. Theoretically, the effects of confinement potential [4,19] and degeneracy [23, 24] are studied on electron-electron interactions and plasmons, by knowing the fact [1] that plasmons gives reasonably accurate information about the nature and structure of the material through which they propagate. Calculated plasmons are directly compared directly with the experimental findings [11]. Also, the XC- functionals are compared with the available LRDMC [21, 22] data.

In section 2, wire model and details of confinement potential models are given. Theoretical method is presented in section 3, results and discussion are in section 4 followed by conclusion in section 5.

2 Wire Model

Here, the single band model is considered. The Hamiltonian for such a system in second-quantization takes the form as[23, 24]

$$
H = \sum_{k\sigma} \epsilon_{k\sigma} a_{k\sigma}^{\dagger} a_{k\sigma}
$$
$$
+ \frac{1}{2} \sum_{k_1,k_2,q,\sigma_1\sigma_2} \langle k_1 + q, k_2 + q|V(q)|k_1 : k_2 \rangle \quad (1)
$$
$$
a_{k_1+q,\sigma_1}^{\dagger} a_{k_2-q,\sigma_2}^{\dagger} a_{k_2\sigma_2} a_{k_1}\sigma_1,
$$

where $\epsilon_{k\sigma} = \hbar^2 k^2/2m^*$ (with band effective mass m^*), $a_{k\sigma}^{\dagger}$ and $a_{k\sigma}$ are creation and annihilation operators. $V(q)$ is the Coulomb interaction potential (electron-electron ($e - e$) interactions) for wire electrons in q-space. In this model, band interpretation is assumed to be done by changing the spin degeneracy factor g_s. In degenerate state ($g_s = 2$) , up-spin and down-spin components are equal while in non-degenerate state ($g_s = 1$) there is an imbalance between up-spin and down-spin components. In quasi-1D wire, Au atoms are modeled as homogeneous gas of electrons embedded in a rigid positive charge background in order to maintain charge neutrality. Electrons are free to move along the length of the wire $i.e$ x-axis while their motion is confined quantum mechanically in the yz-plane. The electrons are supposes to occupy only the lowest energy sub-band in yz-plane due to strong quantum confinement shown schematically in figure 2. Here, parabolic
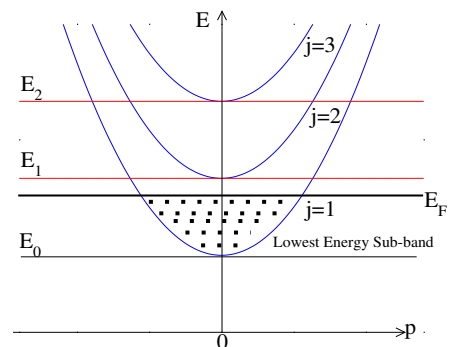
Fig. 2 The total energy E vs the in-layer momentum p of a 2DEG. E_F is the Fermi energy, j is the sub-band index, and E_1 and E_2 are the discrete energy levels along the quantization direction. Here, only the lowest energy sub-band is shown to be occupied.

energy sub-band dispersion is considered with an assumption that all complicated band structure effects are represented through the band effective mass m^*. These assumptions are quite reasonable for 1D electrons as realized in metallic atomic chains. Therefore, the one-electron wave function in this model is defined as

$$\Psi_k(r) = L^{-1/2} e^{\iota k z} \Phi(r_\perp), \qquad (2)$$

where L is the length of the wire and $\Phi(r_\perp)$ is the transverse part of the total wave function with $r_\perp$ being the projection of the three dimensional vector r on the transverse plane. Quasi-1D wires corresponds to non-vanishing $\Phi(r_\perp)$, while in clean-1D wires it vanishes. The Coulomb interaction potential in its Fourier transform is defined as

$$V(q) = \frac{e^2}{\epsilon_0} \int_{-\infty}^{\infty} d(z-z') \, e^{\iota \, q(z-z')}$$
$$\int dr_\perp \, dr'_\perp \frac{|\Phi(r_\perp)|^2 \, |\Phi(r'_\perp)|^2}{[(z-z')^2 + (r_\perp - r'_\perp)^2]^{1/2}}, \qquad (3)$$

where e is the electronic charge and ϵ_0 is the dielectric constant of the background material.

2.1 Harmonic Confinement (HC)[4]:

In the yz-plane, the wire electrons are modeled by a symmetric 2D harmonic potential as

$$V_c(r_\perp) = \hbar^2 r_\perp^2 / (8 m^* w^4), \qquad (4)$$

with w the transverse width of the wire. In the lowest energy sub-band $\Phi(r_\perp)$ takes the form as

$$\Phi(r_\perp) = (2\pi w^2)^{1/2} e^{(R^2/4w^2)}, \qquad (5)$$

putting the value of $\Phi(r_\perp)$ in the integral of Eq. (3), $V(q)$ can be evaluated as

$$V(q) = \frac{e^2}{\epsilon_0} E_1(q^2 w^2) \exp(q^2 w^2), \qquad (6)$$

with $E_1(qw)$ being the exponential-integral function.

2.2 Infinite Square Well Confinement (ISWC)[19]:

In the yz-plane, $V(q)$ is obtained numerically as

$$V(q) = \frac{2e^2}{\epsilon_0} \int_0^a dy \int_0^a dy' \int_0^a dz \int_0^a dz' |\phi(y,z)|^2$$
$$\times |\phi(y',z')|^2 K_0 \left(q\sqrt{(y-y')^2 + (z-z')^2} \right) \qquad (7)$$

with

$$\Phi(y,z) = (\frac{2}{a}) sin(\frac{\pi y}{a}) sin(\frac{\pi z}{a}), \qquad (8)$$

where K_0 is the zeroth-order modified Bessel function of the second kind and a is the width of the square well. In case of intra-wire $e-e$ interactions $V(q)$ takes the form as

$$V(q) = \frac{2e^2}{\epsilon_0} K_0(qw). \qquad (9)$$

While in case of inter-wire $e-e$ interactions (although not considered here) the above equation can be modified as

$$V_{ll'}(q) = \frac{2e^2}{\epsilon_0} K'_0(q\sqrt{w^2 + (1-\delta_{ll'})d^2}), \qquad (10)$$

here l and l' are the wire indices of two parallel wires and $K'_0(x)$ is the zeroth-order modified Bessel's function of the first kind. It can be predicted here that, at very small d (center-to-center wire separation), $V_{ll'}(q)$ can give more accurate information about the nature and splitting of 1D-band (much progress has already been done).

3 Theoretical Method

Dielectric formulation has been used in this work, where the calculations of dynamical susceptibility $\chi(q,\omega)$ is important. The poles of $\chi(q,\omega)$ gives the account of electrostatic excitation energy $i.e.$ $\omega_p(q)$. However, the many-world nature of the system forbids exact calculation of $\chi(q,\omega)$, therefore, some approximation has to be made. Here, $\chi(q,\omega)$ is determined by employing the random phase approximation (RPA) [5] within the framework of linear response theory and is given as

$$\chi(q,\omega) = \frac{\chi_0(q,\omega)}{1 - V(q)\chi_0(q,\omega)}, \qquad (11)$$

where

$$\chi_0(q,\omega) = -\frac{2}{\hbar} \int_{-\infty}^{\infty} \frac{dp}{h} \frac{f^0(p + \hbar q/2) - f^0(p - \hbar q/2)}{\omega - pq/m^* + \iota \eta}. \qquad (12)$$

Take $\hbar = 1$ and put $(p - q/2) = k$ in above Eq. we get

$$\chi_0(q,\omega) = -\frac{1}{\pi} \int_{-\infty}^{\infty} dk \frac{f^0(k+q) - f^0(k)}{\omega - \frac{q}{m^*}(k + \frac{q}{2}) + \iota \eta}, \qquad (13)$$

substitute $k + q = k'$ in first term of the above expression and after solving with $f^0(p) = \Theta(k_F - k)$ (step function at $T = 0K$), we get

$$\chi_0(q,\omega) = \int_0^{k_F} \frac{dk}{2\pi} \left[\frac{-2(kq/m^* - q^2/2m^*)}{\omega^2 - (kq/m^* - q^2/2m^*)^2} \right.$$
$$\left. + \frac{2(kq/m^* + q^2/2m^*)}{\omega^2 - (kq/m^* + q^2/2m^*)^2} \right]. \tag{14}$$

Integrating Eq.(14), we get

$$\chi_0(q,\omega) = \frac{m^* g_s}{2\pi q} \ln \left| \frac{\omega^2 - \omega_-^2}{\omega^2 - \omega_+^2} \right|, \tag{15}$$

this $\chi_0(q,\omega)$ is the Hartree-Fock dynamical susceptibility of non-interacting electrons with

$$\omega_\pm = \frac{qk_F}{m^*} \pm \frac{q^2}{2m^*}, \tag{16}$$

here $\omega_\pm$ corresponds, respectively, to the upper and lower boundary of the (single) electron–hole pair continuum. In the RPA, we address the local correlations between two electrons *via* bare $V(q)$ which takes in to account full screening in the system. In Eq. (16), $k_F(= \pi n/g_s)$ is the 1D Fermi wave vector through which g_s comes in to picture. Further, the electrostatic excitation energy $\omega_p(q)$ is obtained readily from the poles of Eq. (11) as

$$1 - V(q)\chi_0(q,\omega) = 0 \tag{17}$$

$$1 - V(q)\left(\frac{m^* g_s}{2\pi q}\right) \ln \left| \frac{\omega^2 - \omega_-^2}{\omega^2 - \omega_+^2} \right| = 0 \tag{18}$$

$$\omega_p(q) = \sqrt{\frac{\omega_-^2 - \omega_+^2 e^{\mathcal{O}(q)}}{1 - e^{\mathcal{O}(q)}}} \tag{19}$$

with

$$\mathcal{O}(q) = \frac{2\pi q}{m^* g_s V(q)}. \tag{20}$$

Next, the fluctuation-dissipation theorem [23] relates the imaginary part of $\chi(q,\omega)$ with static structure factor $S(q)$ as

$$S(q) = -\frac{1}{\pi n} \int_0^\infty d\omega Im\chi(q,\omega), \tag{21}$$

here, n is the linear electron number density. With the knowledge of $S(q)$, the total energy E_T (per particle) of electrons can be calculated as[24]

$$E_T = \frac{P_F^2}{6m^*} + \int_0^{e^2} d\lambda \frac{E_{int}(\lambda)}{\lambda}, \tag{22}$$

here, first term is the non-interacting kinetic energy while the second term gives the account of exchange-correlation energy E_{xc} with

$$E_{int}(\lambda) = \int_0^\infty \frac{dq}{2\pi} V(q,\lambda)[s(q,\lambda) - 1], \tag{23}$$

in above, $V(q,\lambda) = \lambda f(qw)/(2\epsilon_0)$. λ being the coupling constant and $f(qw)$ (see appendix) is the form factor. E_{xc} accounts for the electronic energy other than non-interacting kinetic and electrostatic energy contributions. Further, the correlation energy E_c can be obtained by subtracting the exchange energy E_x from the second term of Eq.(22). E_x can be obtained from Eq. (23) by replacing $S(q,\lambda)$ with the Hartree–Fock structure factor $S_0(q)(= q/2)$ which is λ independent. In the next section, the numerical results of $V(q)$, $\omega_p(q)$ and XC-functionals are shown at g_s=2 and g_s=1 with extra effects of confinement potentials on $V(q)$ and $\omega_p(q)$.

4 Results and Discussion

In this section, the numerical results are presented for wire parameters which are pertinent to the experimentally fabricated wires. Unless otherwise specified, units used are:, $\omega_p(q)$ in E_F, q in Å^{-1} and w in Å. Quasi-1D wire is characterized by the effective density parameter $r_s^*(= 1/2na_0^*)$; a_0^* is the effective Bohr atomic radius. For brevity, it is assumed that system is at $T = 0K$, though experiments are performed at finite temperature T. This assumption seems to be quite reasonable, as k_BT/E_F is of the order of 10^{-2} for Au chain at $T = 300K$. Large Fermi velocity corresponding to room T can be achieved by tuning r_s^* parameter (effective coupling). For experimental point of view, the used RPA gives good agreement with experimental data in high density regime $(0 < r_s^* < 1)$. This section includes, general wire models, experimental comparison and XC-functionals as sub-sections.

4.1 General Wire Models

The g_s-dependence of $V(q)$ vs q at $w = 4$ and $r_s^* = 0.62$ is shown in figure 3. $V(q)$ is found to have considerable dependence on the degeneracy factor even at $q \to 0$. For $g_s = 2$, the slope of the interaction curve is larger than $g_s = 1$, indicating that the extent of $e - e$ interactions is more in degenerate state where up-spin and down-spin components are equal. In figures 4(a) and (b), the variation of $V(q)$ in two different confinement models is shown at $g_s = 1$ and $g_s = 2$, respectively. It is clear that $V(q)$ depends strongly on the nature of the confinement potential. The infinite square-well confinement (ISWC) results in somewhat harder $e–e$ interaction as compared to the harmonic confinement (HC) and effect of both is much harder at $g_s = 2$ (figure 4(b)). Also, the difference between the results is slightly more at $g_s = 1$ (figure 4(a)). Significantly, it is observed that $V(q)$ depends effectively on both the confinement models over
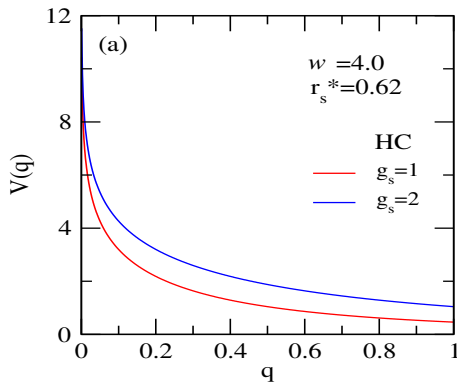
Fig. 3 The variation of $V(q)$ with q at $w = 4$ and $r_s^* = 0.62$ for $g_s = 1$ and $g_s = 2$ in HC model.

the q-range which is accessible to inelastic scattering experiments $i.e (0 < q \approx 0.12)$ [11]. The study of band and confinement interpretation of $V(q)$ is worth in order to calculate other exchange-correlational properties of quasi-1D wires in this q-range. Here, q is restricted within a proper cut off value ($q_c \approx 2 - 3$) to make this model consistent with the assumed single band model [23, 24].

To elucidate the role of band and confinement interpretation, the results of $\omega_p(q)$ are compared in figure 5. The numerical values of $\omega_p(q)$ are obtained from the
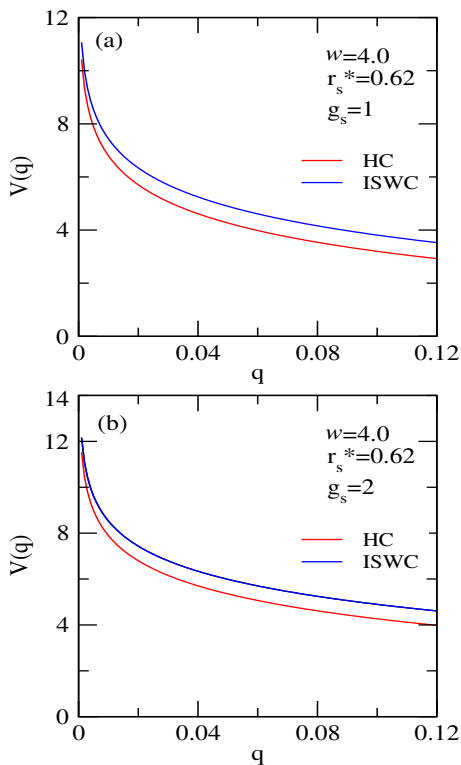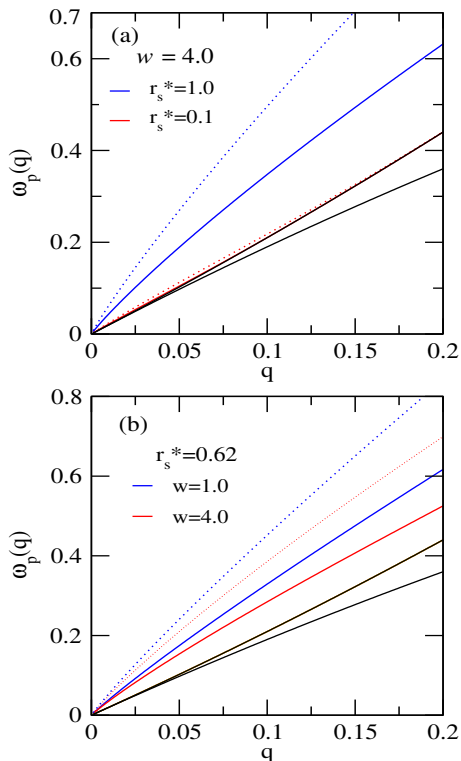
poles of $\chi(q, \omega)$ in eq. (11). The harder confinement (ISWC) causes a blue-shift in $\omega_p(q)$ $w.r.t$ HC model in both states, which increases monotonically with q. The magnitude of the shift is seen to be slightly increased at $g_s = 2$ than $g_s = 1$. This blue-shift in energy is associated with stronger exchange-correlations among electrons under the influence of ISWC. Interestingly, switching from $g_s = 2$ to 1 cause red-shift in both the models. This indicates the weakening of XC-effects at $g_s = 1$. Therefore, as an important finding, it is observed that within the bare local potential $V(q)$ (without any non-local corrections), the extent of exchange-correlations can be modified by doing the band and confinement interpretation of system electrons. In fig-
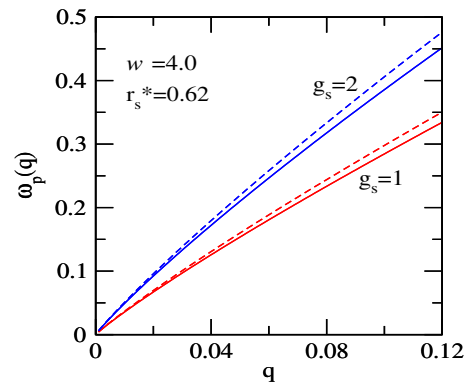

Fig. 5 The variation of $\omega_p(q)$ with q at $w = 4$ and $r_s^* = 0.62$ for $g_s = 1$ (red lines) and $g_s = 2$ (blue lines) in HC (solid lines) and ISWC (dashed lines) models.

ure 6(a), r_s^*-dependence of $\omega_p(q)$ is depicted at fixed width of wire. The energy of $\omega_p(q)$ also increases with increase in r_s^* for both degenerate and non-degenerate states. Increase in energy is attributed to the fact that at high r_s^*, $e - e$ correlations increases and electrons oscillate collectively with large frequency. Increased $e - e$ correlations bring about more potential energy among system electrons which reflects in their collective excitation spectra i.e $\omega_p(q)$ at high r_s^*. It is well checked that, at both (or all) densities, the energy of these oscillations is found to be increased at $g_s = 2$, but the quantitative effects of degeneracy parameter are more at low densities (high r_s^*). In figure 6(b), the wire width dependence of $\omega_p(q)$ is shown at fixed r_s^*. Dependence of w is found to be in contrast with r_s^*-dependence. There is loss in energy of $\omega_p(q)$ with increase in w at both $g_s = 1$ and 2. On the lift of degeneracy, energy of $\omega_p(q)$ is found to be decreased at both (or all) w-values. Therefore, decrease in w and increase in r_s^* cause qualitatively same effect on $e - e$ interactions irrespective to the confinement model. It is also noted that calculated $\omega_p(q)$ at indicated wire parameters lies above the

Fig. 4 $V(q)$ vs q at $w = 4$, $r_s^* = 0.62$ in HC and ISWC models for $g_s = 1$ [in panel (a)] and $g_s = 2$ [in panel (b)].

Fig. 6 The dependence of $\omega_p(q)$ on r_s^* [in panel (a)] and w [in panel (b)] at indicated wire parameters for $g_s = 1$ (solid lines) and $g_s = 2$ (dotted lines) in HC model. The thick black lines represent the boundaries of the single electron–hole (e-h) pair continuum at $r_s^* = 0.1$ [in panel (a)] and at $w = 4.0$ [in panel (b)].


Fig. 7 The dependence of $\omega_p(q)$ on q for indicated wire parameters at $g_s = 1$ (solid lines) and $g_s = 2$ (dotted lines) in ISWC model. The thick dash–dotted lines represent the boundaries of the single electron–hole (e-h) pair continuum at $r_s^* = 1.0$ [in panel (a)] and at $w = 2.0$ [in panel (b)].

e-h pair continuum and plasmons can be measured experimentally [7,24]. For the purpose of generalization of this model, the results of $\omega_p(q)$ for an other set of system parameters are plotted in figure 7 along with e-h continuum in ISWC model. At large w and high r_s, the results obtained are in qualitative agreement with the results shown in figure 6. For large-q range, it is found that at a certain q, $\omega_p(q)$ merges to the single particle e-h pair continuum. It is also noted that, while solving Eq.(11) for $\omega_p(q)$, multiple roots have been observed with equal stand probability inside and outside of the e-h pair continuum. Only those values of $\omega_p(q)$ are opted which lies above the upper boundary of e-h pair continuum [7]. Here, in both states $g_s = 1$ and 2, $\omega_p(q)$ lies above the upper boundary of e-h pair continuum. Thus, one can say that metallic behaviour of electrons in single quasi-1D wire is possible in both $g_s = 1$ and 2 states even at $T = 0K$ which is in contrast to the findings of Ahn *et al.* [17] observations. At $g_s = 1$, such metallic behaviour can be completely understood by virtue of the imbalance between spin-components. While in degenerate state, dominating XC-effects are responsible for metallic behaviour of electrons. Thus,
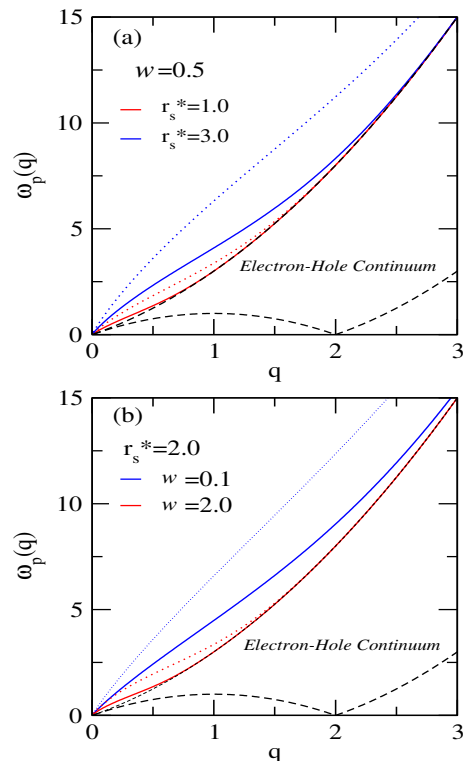
the study of XC-functionals is very important in order to understand the exact nature of 1D-bands.

4.2 Experimental Comparison

To enable a direct comparison with the experimental data [11], the used wire parameters appropriate to the
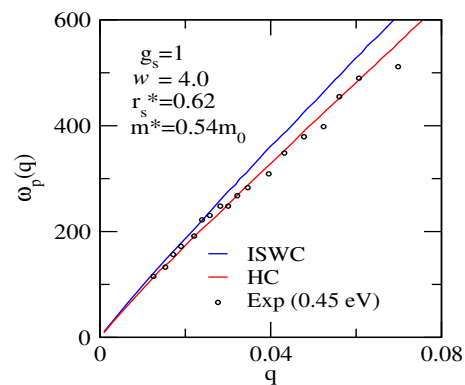

Fig. 8 The variation of $\omega_p(q)$ (meV) vs q at indicated wire parameters in HC and ISWC models. The symbols are the experimental data of Nagao *et al.* [11] for electron beams having incident energy of $45eV$.

Au chain on the Si(557) surface are: $\epsilon_0 = (1 + \epsilon_{Si})/2$, with $\epsilon_{Si} = 11.5$, $k_F = 0.41$ Å^{-1}, w= 4 Å and $g_s = 1$. On experimental lines, only intra-wire interactions are taken in to account by setting degeneracy factor equal to unity. The numerical results of $\omega_p(q)$ (in meV) vs q are plotted at $w = 4$, $r_s^* = 0.62$ and $m^* = 0.54m_0$ for both HC and ISWC models in figure 8. In the RPA, by using above wire parameters the HC model data of $\omega_p(q)$ exhibits very good agreement with the experiments data of $\omega_p(q)$ obtained by electron-energy-loss spectroscopy (EELS) at incident energy of $45eV$. At $g_s = 1$, reasonably good agreement have been obtained at $m^* = 0.54m_0$: a value close to $0.45m_0$ determined by PES [18] ; m_0 is the free electron mass. For these agreed values of g_s and m^*, calculated $r_s^* = 0.62$ and $a_0^* = 11.57a_0$; a_0 is the Bohr atomic radius. This calculated value of m^* obtained by fitting the EELS data in the RPA, deviates from the PES results [18] while in close agreement with the theoretical findings of Nagao $et\ al$ [11]. Conceivably, this departure of m^* arise due to the fact that these two experiments (PES and EELS) works in different k-states of the band and having different masses of incident particles. In PES, m^* reflects the band curvature at low k-states near minimum, while in EELS, it reflects the same at higher k-states. In EELS experiments, electrostatic oscillations are composed of electronic transitions near the Fermi level and reflect the band dispersion near E_F. The study of $\omega_p(q)$ in this region, requires the incorporation of XC-effects on obligatory basis. Here XC-effects are already included through RPA, but m^* departure is still there which is more in case of ISWC model. It is found that difference in m^* is because of the fact that plasmons incorporate the effect of exchange-correlations in addition to the band effective parameters (degeneracy:g_s and confinement potential: $V(q)$). By adjusting these parameter a good fit can be obtained between theoretical and experimental data. In Table 1, band fitting parameters of 1D Au wire are given in order to see whether a close agreement with data close to $m^* = 0.45m_0$ can be achieved. The values of $\omega_p(q)$ corresponding to $g_s = 2$ matches the experimental data at a somewhat higher m^* i.e $0.57m_0$ even in HC model. It is also clear from tabulated data that, by choosing a sufficiently larger

Table 1 Band fitting parameters of Au wire at fixed n and w.

Conf.	n(Å)	g_s	$\frac{w}{Å}$	r_s^*	$\frac{m^*}{m_0}$	$\frac{a_0^*}{a_0}$
HC	0.13	1	4.0	0.62	0.54	11.57
HC	0.13	2	4.0	0.33	0.57	10.96
ISWC	0.13	1	4.0	0.68	0.59	10.59
ISWC	0.13	2	4.0	0.47	0.82	07.62

m^*, $\omega_p(q)$ for ISWC model can be brought closer to the experimental data for both $g_s = 1$ and 2. Therefore, the effective study of plasmons in 1D wires requires the sound knowledge of band effective parameters along with the technique used to include XC-effects. On the other hand, the value of $m^* = 0.54m_0$ is very close to the theoretically calculated value of $m^* = 0.52m_0$ by including the effects of non-local corrections (or dynamics of XC-effects) [11]. This implies that the proposal of band and confinement interpretation is also capable of incorporating exchange-correlations well within the RPA. Next, the modified single e–h pair continuum
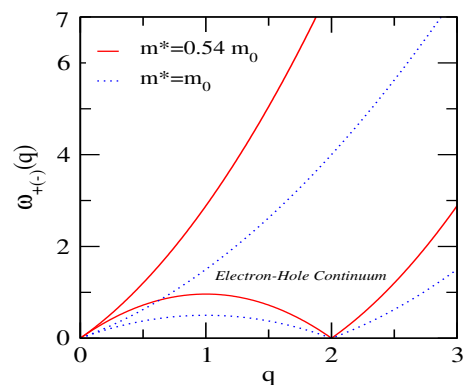
Fig. 9 e-h pair continuum at $m^* = 0.54m_0$ (red solid lines) and $m^* = m_0$ (blue dotted lines).

is shown in figure 9, at $m^* = 0.54m_0$ and $m^* = m_0$ for $w = 4$ and $r_s^* = 0.62$. At $m^* = 0.54m_0$, the e-h pair continuum oscillates with the higher energy than $m^* = m_0$. This is due to the fact that, when degeneracy is lifted î.e $g_s = 1$ electrons shifts to higher k-bands leaving behind a hollow positive place at low k-bands. Antiparticles (holes) at low k-bands having less kinetic energy (velocity) than the electrons at higher k-bands. Therefore, one can directly assigned this increased m^* to the mass of holes which is responsible for greater XC-effects in the system.

4.3 Exchange-Correlation Functionals

Although, after having reasonably good agreement with experimental data of Ngao $et\ al.$, their ad-hoc idea of spin-orbital splitting of 1D-band is not accepted, theoretically. Because they have not proved it rigorously. It is found here that the interplay between band effective parameters and XC-functionals can explain splitting of bands in quasi-1D wires in a better way. Because, in order to add spin-orbital coupling parameters in any ab-$initio$ [16] calculations, the exact form of XC-functionals is required which helps in formulating the

XC-potential $V_{xc}(r)$ [25] as

$$V_{xc}(r) = \frac{\delta E_{xc}(r)}{\delta \rho(r)}, \qquad (24)$$

here, E_{xc} is the exchange-correlation energy and $\rho(r)$ is the local electronic charge density. The exact value of E_{xc} is difficult to calculate: approximations have to be made at that point. Here, E_{xc} is calculated from Eq. (22) by putting the value of $S(q)$ (from Eq. (21)) in Eq. (23) within the RPA. The numerical results of E_{xc} for $g_s = 2$ and $g_s = 1$ of quasi-1D wire are listed in Table 2, at $w = 1$ for some representative values of r_s^* along with LRDMC data of Casula *et al.*[21]. It is found that the

Table 2 E_{xc} (in $Ryd.^*$/electron) for $w = 1$ in RPA along with LRDMC (parentheses) data.

r_s^*	$g_s = 2$	$g_s = 1$
0.2	-0.751974	-0.804191
	(-0.804759)	(-0.804628)
0.4	-0.67644302	-0.751144
	(-0.675751)	(-0.751468)
0.6	-0.62302827	-0.708838
	(-0.620978)	(-0.708889)
0.8	-0.58325853	-0.673537
	(-0.579186)	(-0.673040)
1.0	-0.55272631	-0.643393
	(-0.546211)	(-0.642101)

magnitude of E_{xc} increases with increasing r_s^* in both the spin states i.e., $g_s = 2$ and $g_s = 1$. This implies that with increase in r_s^* (directly proportional to m^*), E_{xc} increases due to enhancement in m^*. Greater mass of interacting particles give rise to greater XC-effects in the system (discussed in sub-section 4.2). Further, the magnitude of E_{xc} is found to be increased at $g_s = 2$ than $g_s = 1$ (see table 2) at fixed r_s^*. These findings of E_{xc} are in both qualitative and quantitative agreement with available LRDMC data at $w = 1$. For experimentally achievable width of wire ($w = 4$), the numerical results of E_{xc} for $g_s = 2$ and $g_s = 1$ are listed in Table 3 and the qualitative behaviour is same as discussed for $w = 1$ in Table 2. The kinetic energy $E_{K.E}$ calculated from first term of Eq.(22) is also shown in figures 10.

Table 3 E_{xc} (in $Ryd.^*$/electron) for $w = 4$ in the RPA along with LRDMC (parentheses) data.

r_s^*	$g_s = 2$	$g_s = 1$
0.2	-0.209480	-0.214308
0.4	-0.201382	-0.209433
0.6	-0.194686	-0.205107
0.8	-0.188950	-0.201203
1.0	-0.183942	-0.197628
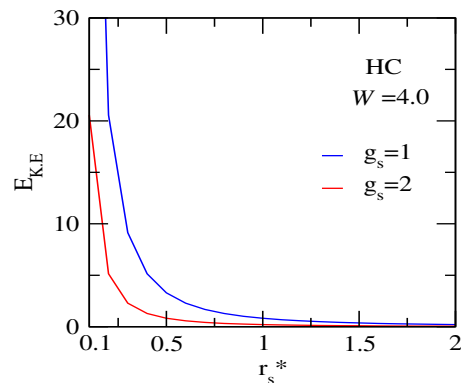
Fig. 10 The r_s^*-dependence of $E_{K.E}$ at $w = 4$ in HC model.

The r_s^*-dependence of $E_{K.E}$ depicts that the kinetic effects are more pronounced at $g_s = 1$ than $g_s = 2$. In both situations, the $E_{K.E}$ decreases with increase in r_s^* and finally becomes zero at sufficiently high value of r_s^*, which is different for $g_s = 2$ and $g_s = 1$. At that particular value of r_s^* (usually high), the XC-effects dominates over kinetic effects and as a consequence of which there is a mass-asymmetry among system electrons near Fermi-level. At E_F, this mass-asymmetry leads to the splitting of 1D-bands and gives a different way to understand band-splitting without ah-hoc SO-coupling. Among two splitted 1D-bands, one lies above
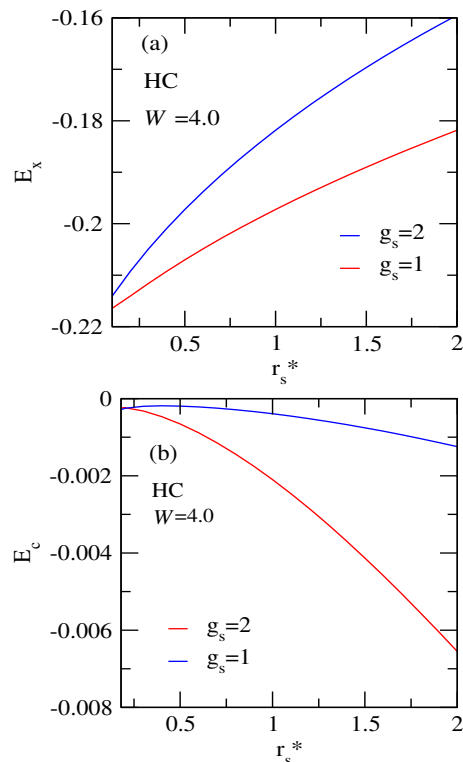
Fig. 11 The r_s^*-dependence of E_x [in panel (a)] and E_c [in panel (b)] at $w = 4$ in HC model.

E_F and other below E_F. Theoretically on the basis of band picture (see figure 2), it can be predicted that the electrons in the band below E_F are heavier than the electrons in the band above E_F. Relating these predictions to the assumed intra-wire interactions it is obvious to say that both bands belongs to the same single wire on $Si - Au$ surface. Now, according to this work the observed peaks in experiments [11, 15] can also belongs to a single wire. Simultaneously, these peaks can also associates to the different particles in that same wire on the basis of mass-asymmetry among them. Higher peak associates with the lighter electrons at the surface while the lower peak belongs to the heavier electrons at step-edge in the same wire. Therefore, this work supports the experimentally detection of step-edge electrons by Ahn *et al.*[17] in quasi-1D wires. It is the mass-asymmetry of carrier in the wire which is responsible 1D-band splitting when XC-effects are dominant.

Further, the overall behaviour of XC-functionals are decided by its two components i.e. E_x and E_c. In figures 11(a) and (b), respectively, the r_s^*-dependence of E_x and E_c is depicted. At fixed r_s^*, the magnitude of E_x is less for $g_s = 1$ as compared to $g_s = 2$. On the other hand at $g_s = 1$, the magnitude of E_c is more as compared to $g_s = 2$. The calculated results of E_c are in both quantitative and qualitative agreement with the available LRDMC data of Shulenberger *et al.* [?] shown in table 4. Next, in order to study instability

**Table 4** E_c (in $Ryd.^*$/electron) for $w = 4$ in RPA along with LRDMC (parentheses) data.

r_s^*	RPA	$LRDMC$
0.2	-0.000232	-0.000112
0.4	-0.000466	-0.000403
0.6	-0.000885	-0.000827
0.8	-0.001437	-0.001349
1.0	-0.002098	-0.001949

criterion, only one splitted 1D-band is considered with polarization factor: $\zeta = (n_\uparrow - n_\downarrow)/n$, where $n_\uparrow(n_\downarrow)$ being the density of up (down)-spin components. Here, $\zeta = 0$ $(g_s = 2)$ and $\zeta = 1$ $(g_s = 1)$ represent, respectively, the unpolarized and fully-polarized states. Starting from $\zeta = 0$ and moving towards $\zeta = 1$, the imbalance of spin-components increases, due to which the kinetic energy increases (see figure10) and exchange-correlation energy decrease (see Table 2). The competition between these two tendencies may leads to charge or spin instabilities in these systems. On the basis of above calculations it is predicted that such instabilities can occurs in quasi-1D wires when following criterion

is satisfied by the system electrons

$$r_s^*[E_T(\zeta = 1) - E_T(\zeta = 0)] < 0, \qquad (25)$$

here, E_T is the total energy calculated from Eq.(22). The variation of E_T w.r.t r_s^* at $\zeta = 1$ and $\zeta = 0$ is shown in figure 12. It is clear from the figure that E_T
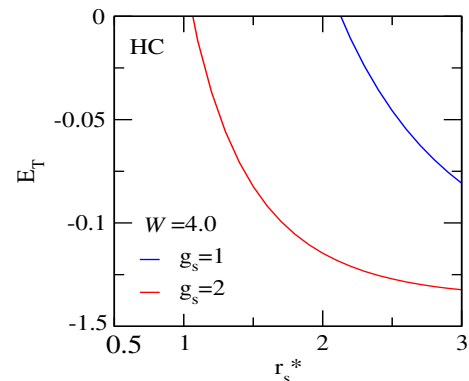
Fig. 12 The r_s^*-dependence of E_T at $w = 4$ in HC model.

becomes negative when XC-effects dominates over kinetic effects. The negativeness of E_T indicates some attractive force among electrons which cause instabilities in these 1D system at particular value of r_s^*. Theoretically, such instabilities can be predicted by calculating the $S(q, \omega)$ as [24]

$$S(q, \omega) = \frac{\hbar}{\pi} Im\chi(q, \omega) \qquad (26)$$

The $S(q, \omega)$ describes the density-fluctuation spectrum of the electron system, and can be measured directly through X-ray inelastic scattering experiments. The value of r_s^* at which the above criterion (Eq. (25)) is satisfied, represented as critical effective electron density r_{sc}^*. Theoretically, r_{sc}^* is difficult to measure in quasi-1D wires and can be further used to calculate critical temperature (T_c). For quasi-1D wires, the fitted formula which relates r_{sc}^* to T_c of is constructed here as

$$T_c = \frac{T}{T_F}; \quad T_F = \frac{\hbar^2}{2m^* k_B} \left(\frac{\pi}{4r_{sc}^* a_0^*}\right)^2. \qquad (27)$$

The exact value of T_c and spin/charge instabilities in quasi-1D wires are still unexplored and demands future investigation. Work related to Eqs. (25), (26) and (27) is in progress as well as the study of plasmons in quasi-1D wires are concerned. These findings are important in order to produce increased energy scale Plasmons in these wires by engineering the band structure and confinement potentials.

5 Conclusions

In conclusion, electrons in HC model serves as a good approximation for theoretical description of the plasmons in atomic scale metal wire at experimentally accessible r_s^* and w. $V(q)$ and $\omega_p(q)$ depends strongly on the confinement model and degeneracy factor. Plasmons are found to relied upon m^*, r_s^* and the nature of the 1D-band. Further, the XC-effects are more significant at high r_s^* and low w. However, their influence grows with increasing confinement and imposing degeneracy in the system. These correlations are found to cause a noticeable energy-shift in $\omega_p(q)$. This implies that band and confinement interpretation of 1D electrons may cause enhanced XC-effects even at high densities and leads to the phenomenon of mass-asymmetry. The exploration of the competition between exchange-correlation functionals gives a better idea about 1D-band splitting over the ad-hoc assumption of SO-coupling. Based on XC-functionals, an instability criterion is proposed, satisfying which a quasi-1D wire may host an (spin/charge) instability at particular T_c. Simultaneously, one can create XC-functionals for quasi-1D wires by mixing and matching given data of exchange and correlation functionals for the purpose of *ab-initio* calculations. Overall these finding may prove useful in fabrication of 1D plasmonic devices like spin transistors, spin filter etc.

6 Appendix 1

In HC, for the calculations of $V(q)$ in Eq.(6), the limiting forms of form factor i.e. $f(qw) = 2E_1(q^2w^2)\exp(q^2w^2)$ are required which can be calculated as

$$f(qw) = \begin{cases} \frac{2}{q^2w^2} & \text{for} \quad (qw \gg 1) \\ \\ 4\ln|\frac{1}{qw}| & \text{for} \quad (qw \ll 1) \end{cases} \quad (28)$$

In ISWC, for the calculations of $V(q)$ in Eq.(9), the limiting forms of the form factor i.e. $g(qw)$ are required which can be calculated as

$$\frac{g(qw)}{\frac{e^2}{\epsilon_0}} = \begin{cases} -2\ln|qw| & \text{for} \quad (qw \ll 1) \\ \\ 2K_0(qw) & \text{for} \quad (1 \ll qw \ll 15) \\ \\ \frac{2}{exp^{qw}}(\sqrt{\frac{\pi}{2qw}}) \times \\ \{1 - (\frac{1}{8qw}) + (\frac{9}{2(8qw)^2}) \\ -(\frac{225}{6(8qw)^3})\} \quad \text{for} \quad (qw \gg 15) \end{cases} \quad (29)$$

Conflicts of interest/Competing interests

Author having no conflicts of interest.

Availability of data and materials

Data and materials available on request from the author.

Code availability

Code for this work is confidential, but may available on written application which includes the description of needs and collaboration with the author.

Authors' contributions

The whole project is designed by Akariti Sharma.

Ethics approval

Not applicable

Consent to participate

Consent is clear and having permission for related research activities.

Consent to publish

Consent is clear for the publication of this work.

References

1. Ting Zhang, Steve Blair, Gray Level Image Encoding in Plasmonic Metasurfaces, Plasmonics 15: 1305–1311 (2020). https://doi.org/10.1007/s11468-020-01151-5.
2. Gao X, Hui Shi J, Shen X, Feng Ma H, Xiang Jiang W, Li L, Jun Cui T, Ultrathin dual-band surface plasmonic polariton waveguide and frequency splitter in microwave frequencies, Appl Phys Lett 102(15): 151912 (2013). https://doi.org/10.1063/1.4802739.
3. Blaber M G, Arnold M D, Ford M J, A review of the optical properties of alloys and intermetallics for plasmonics, J Phys Condens Matter 22(14): 143201 (2010). https://doi.org/10.1088/0953- 8984/22/14/143201.
4. Friesen W I, Bergersen B, Dielectric response of a one-dimensional electron gas, J. Phys. C: Solid State Phys.13, 6627 (1980). https://doi:10.1088/0022-3719/13/36/016.
5. Das Sarma S, Lai W-Y, Screening and elementary excitations in narrow-channel semiconductor microstructures, Phys. Rev. B 32, 1401 (1985). https://doi.org/10.1103/PhysRevB.32.1401.
6. Gold A, Ghazali A, Analytical results for semiconductor quantum-well wire: Plasmons, shallow impurity states, and mobility Phys. Rev. B 41, 7626 (1990). https://doi.org/10.1103/PhysRevB.41.7626.
7. Das Sarma S, Hwang E H, Dynamical response of a one-dimensional quantum-wire electron system, Phys. Rev. B 54, 1936 (1996). https://doi.org/10.1103/PhysRevB.54.1936.
8. Afshin Moradi, Plasmon modes of metallic nanowires including quantum nonlocal effects, PHYSICS OF PLASMAS 22, 032112 (2015). http://dx.doi.org/10.1063/1.4916059.
9. S. Ali, Shafiq Ur Rehman, Z. J. Ding, Stable plasmon excitations in quantum nanowires, PHYSICS OF PLASMAS 25, 082115 (2018).https://doi.org/10.1063/1.5041297.
10. Goñi A R, Pinczuk A, Weiner J S, Calleja J M, Dennis B S, Pfeiffer L N, West K W, One-dimensional plasmon dispersion and dispersionless intersubband excitations in GaAs quantum wires, Phys. Rev. lett. 67, 3298 (1991). https://doi.org/10.1103/PhysRevLett.67.3298.
11. Nagao T, Yaginuma S, Inaoka T, Sakurai T, One-Dimensional Plasmon in an Atomic-Scale Metal Wire, Phys. Rev.Lett. 97, 116802 (2006).https://doi.org/10.1103/PhysRevLett.97.116802.
12. Nagao T, Yaginuma S, Inaoka T, Sakurai T, Jeon D, Sound-Wave-Like Collective Electronic Excitations in Au Atom Chains, J. Phys. Soc. Japan 76, 114714 (2007). https://doi.org/10.1143/JPSJ.76.114714.
13. Liu C, Inaoka T, Yaginuma S, Nakayama T, Aono M, Nagao T, Disappearance of the quasi-one-dimensional plasmon at the metal-insulator phase transition of indium atomic wires, Phys. Rev. B 77, 205415 (2008). https://doi.org/10.1103/PhysRevB.77.205415.
14. Thornton T J, Pepper M, Ahmed H, Andrews D, Davies G J, One-Dimensional Conduction in the 2D Electron Gas of a GaAs-AlGaAs Heterojunction, Phys. Rev. Lett. 56, 1198 (1986) https://doi.org/10.1103/PhysRevLett.56.1198, and Berggren K-F, Thornton T J, Newson D J, Pepper M, Magnetic Depopulation of 1D Subbands in a Narrow 2D Electron Gas in a GaAs:AlGaAs Heterojunction, Phys. Rev. Lett. 57, 1769 (1986). https://doi.org/10.1103/PhysRevLett.57.1769.
15. Losio R, Altmann K N, Kirakosian A, Lin J-L, Petrovykh D Y, Himpsel F J, Band splitting for Si(557)-Au: is it spin-charge separation?, Phys. Rev. lett. 86, 4632 (2001). https://doi.org/10.1103/PhysRevLett.86.4632.
16. Sánchez-Portal D, Riikonen S, Martin R M, Role of Spin-Orbit Splitting and Dynamical Fluctuations in the Si(557)-Au Surface, Phys. Rev. Lett. 93, 146803 (2004). https://doi.org/10.1103/PhysRevLett.93.146803.
17. Ahn J R, Yeom H W, Yoon H S, Lyo I-W, Metal-Insulator Transition in Au Atomic Chains on Si with Two Proximal Bands, Phys. Rev. Lett. 91, 196403 (2003). https://doi.org/10.1103/PhysRevLett.91.196403.
18. Altmann K N, Crain J N, Kirakosian A, Lin J-L, Petrovykh D Y, Himpsel F J, Losio R, Low-dimensional electronic states at silicon surfaces, Phys. Rev. B 64, 035406 (2001).https://doi.org/doi:10.1007/s00339-005-3365-3.
19. Campos V B, Degani M H, Hipólito O,Exchange and Correlation-Effects in a Semiconductor Quantum-Well Wire, Superlatt. Microstruct. 17, 85 (1995). https://doi.org/10.1006/spmi.1995.1018.
20. Robinson I K, Bennett P A, Himpsel F J, Structure of Quantum Wires in Au/Si(557), Phys. Rev. Lett. 88, 096104 (2002). https://doi.org/10.1103/PhysRevLett.88.096104.
21. Michele Casula, Sandro Sorella, Gaetano Senatore, Ground state properties of the one-dimensional Coulomb gas using the lattice regularized diffusion Monte Carlo method, Phys. Rev. B 74, 245427 (2006). https://doi.org/10.1103/PhysRevB.74.245427.
22. Luke Shulenburger, Michele Casula, Gaetano Senatore, and Richard M. Martin, Spin resolved energy parametrization of aquasi-one-dimensional electron gas, J. Phys. A: Math. Theor. 42, 214021 (2008). https://iopscience.iop.org/article/10.1088/1751-8113/42/21/214021/pdf.
23. D. Pines, P. Nozières, The Theory of Quantum Liquids. Benjamin, New York (1966). ISBN-13: 978-0201407747,ISBN-10: 0874809355.
24. See, for example, G. D. Mahan, Many Particle Physics. Plenum Press, New York (1993). ISBN 978-1-4757-5714-9.
25. Kun Cao, Henry Lambert, Paolo G. Radaelli, Feliciano Giustino, Ab initio calculation of spin fluctuation spectra using time-dependent density functional perturbation theory, plane waves, and pseudopotentials, Phys. Rev. B 97, 024420 (2018). https://doi.org/10.1103/PhysRevB.97.024420
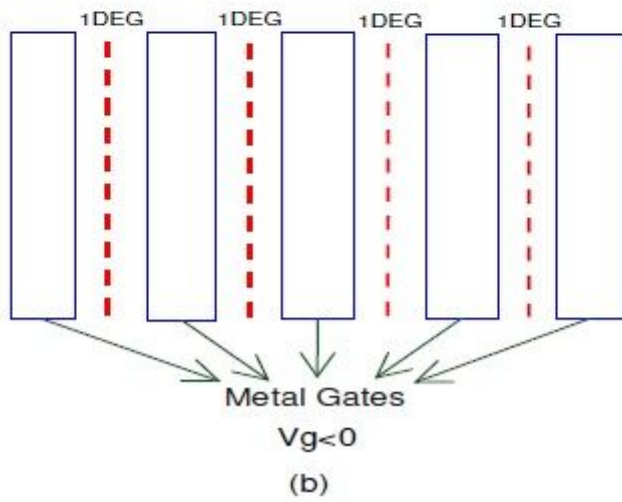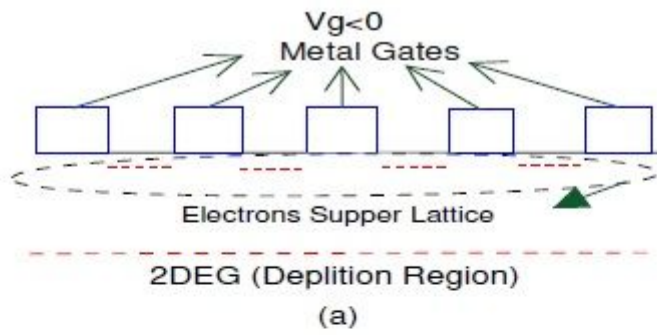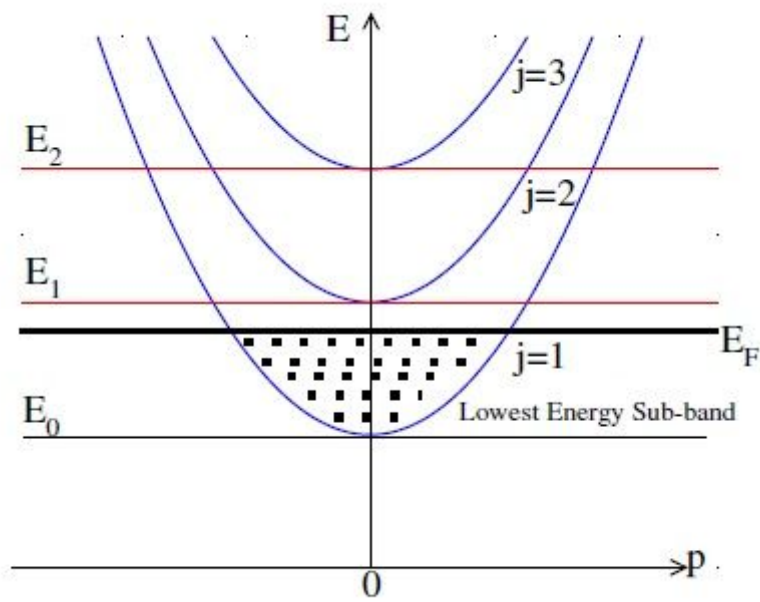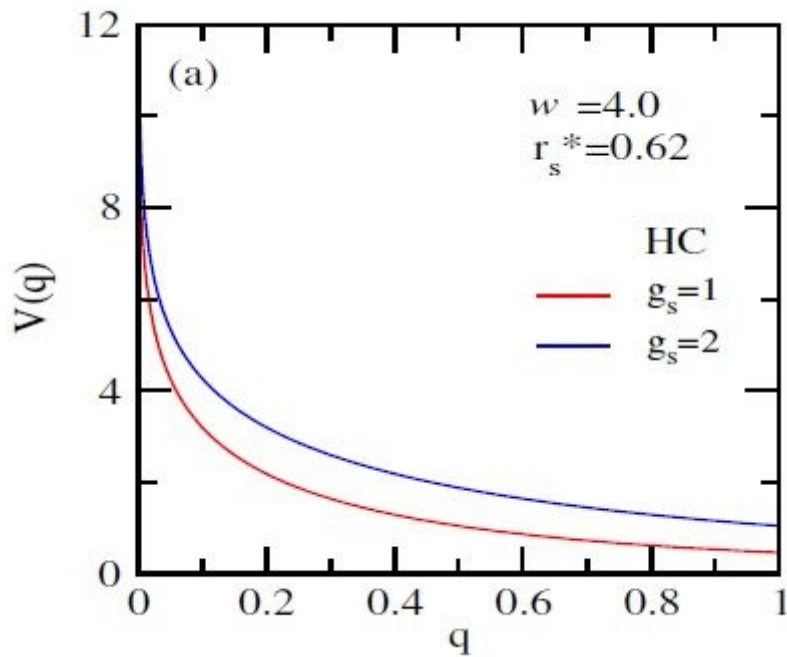
Figures

Figure 1

A set of gates used to form 1D electrons super lattice, lateral view [in panel (a)] and top view [in panel (b)].
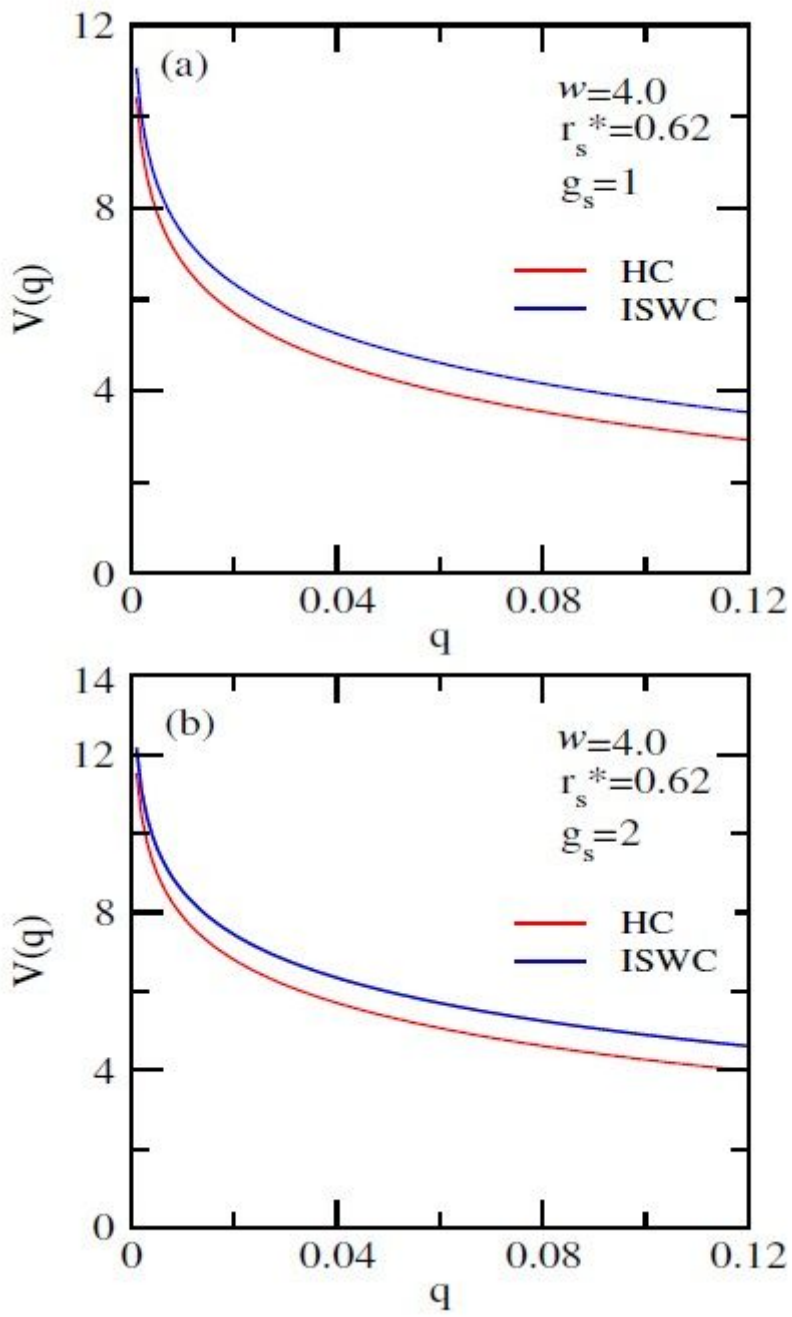
Figure 2

The total energy E vs the in-layer momentum p of a 2DEG. EF is the Fermi energy, j is the sub-band index, and E1 and E2 are the discrete energy levels along the quantization direction. Here, only the lowest energy sub-band is shown to be occupied.
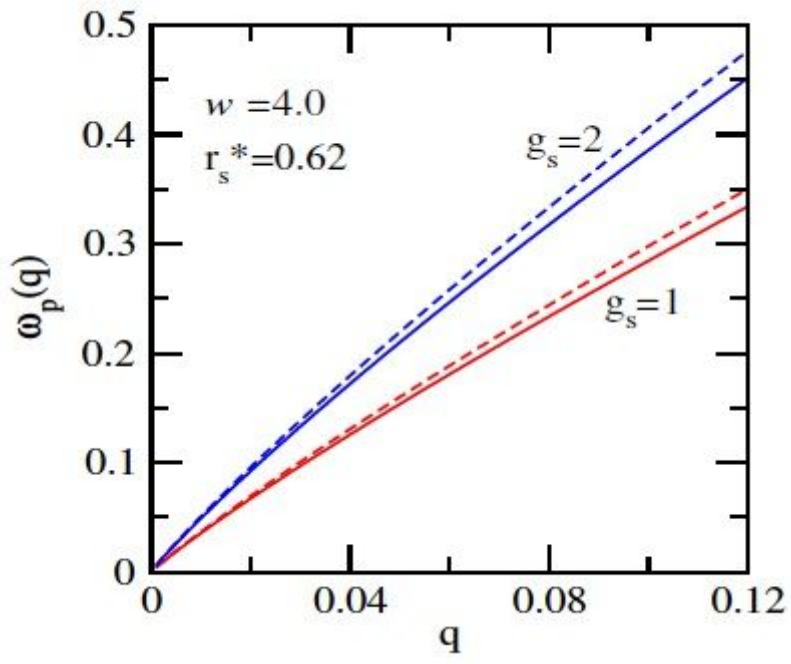

Figure 3

The variation of V (q) with q at w = 4 and r*s = 0:62 for gs = 1 and gs = 2 in HC model.

Figure 4

V (q) vs q at w = 4, r*s = 0:62 in HC and ISWC models for gs = 1 [in panel (a)] and gs = 2 [in panel (b)].

Figure 5

The variation of !p(q) with q at w = 4 and r*s = 0:62 for gs = 1 (red lines) and gs = 2 (blue lines) in HC (solid lines) and ISWC (dashed lines) models.
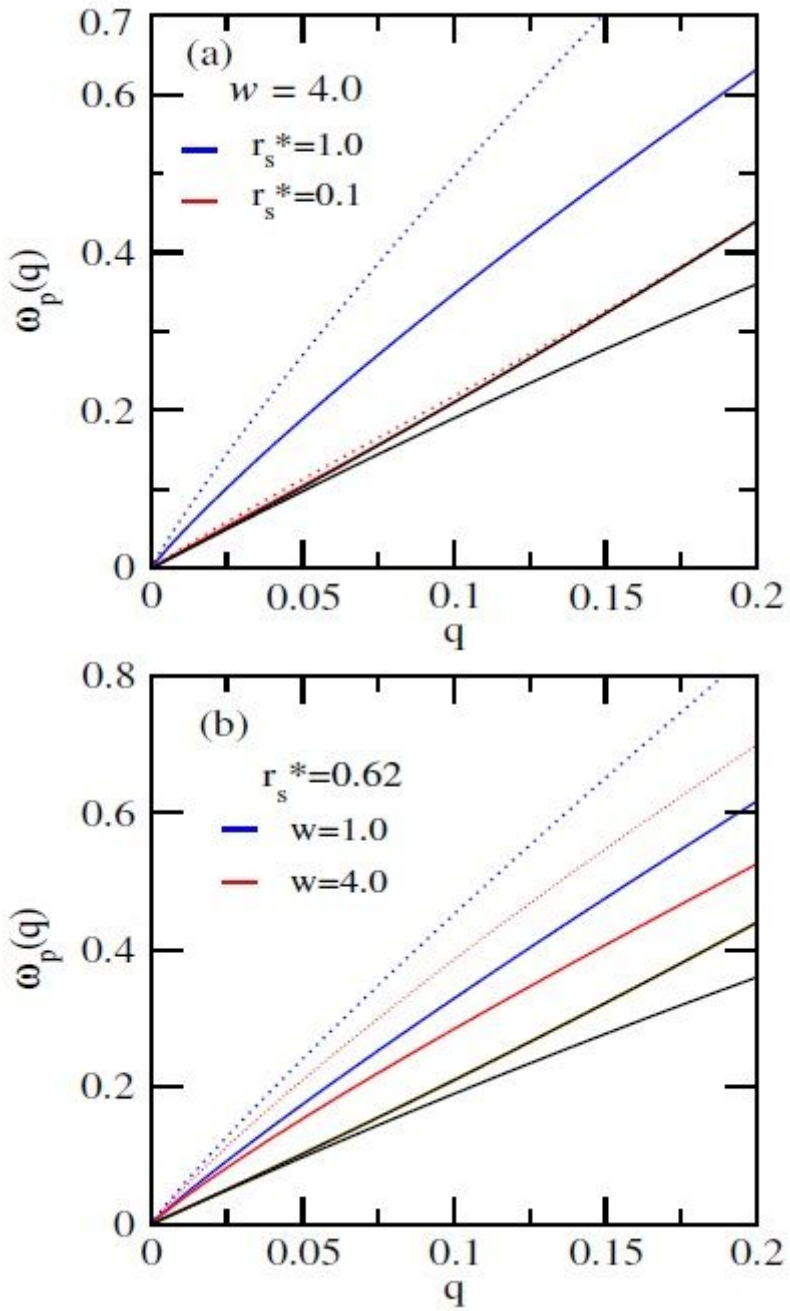
Figure 6

The dependence of !p(q) on r*s [in panel (a)] and w [in panel (b)] at indicated wire parameters for gs = 1 (solid lines) and gs = 2 (dotted lines) in HC model. The thick black lines represent the boundaries of the single electron{hole (eh) pair continuum at r*s = 0:1 [in panel (a)] and at w = 4:0 [in panel (b)].
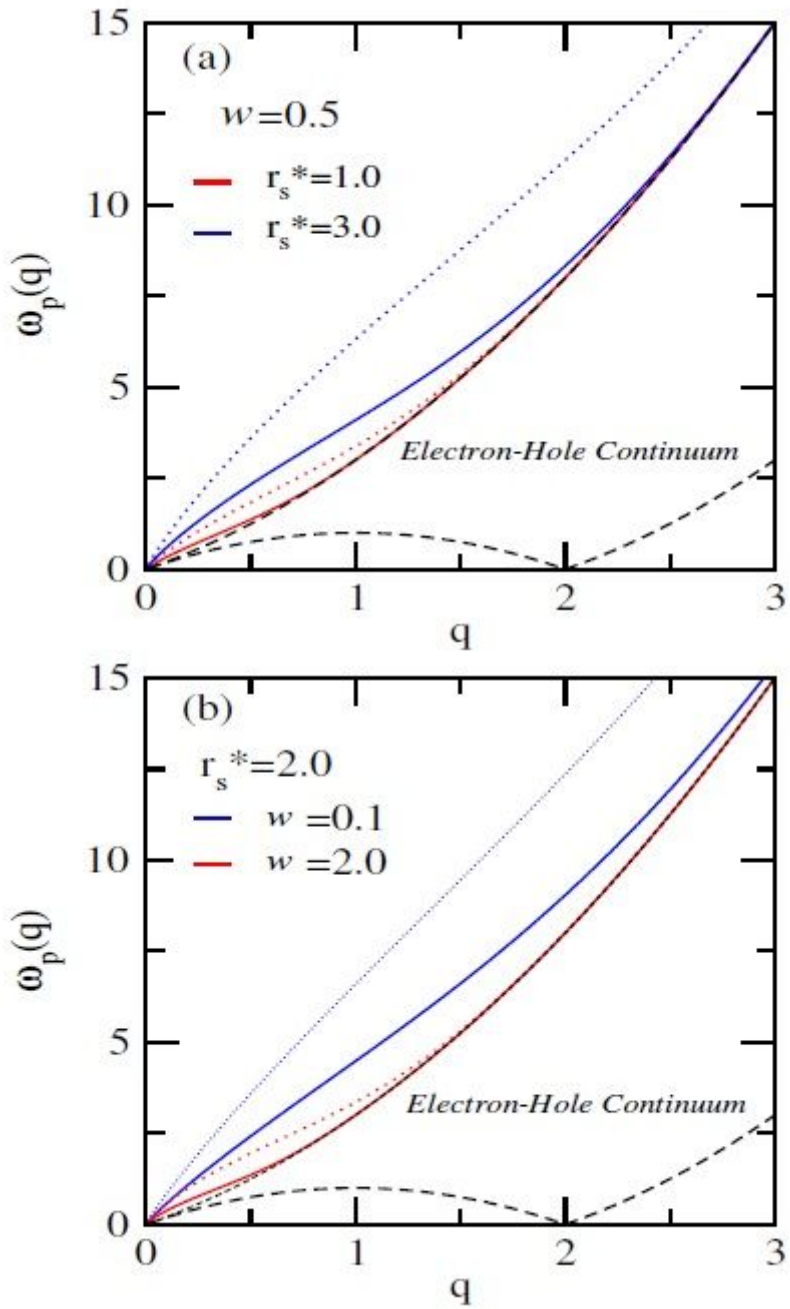
Figure 7

The dependence of !p(q) on q for indicated wire parameters at gs = 1 (solid lines) and gs = 2 (dotted lines) in ISWC model. The thick dash{dotted lines represent the boundaries of the single electron{hole (e-h) pair continuum at r*s = 1:0 [in panel (a)] and at w = 2:0 [in panel (b)].
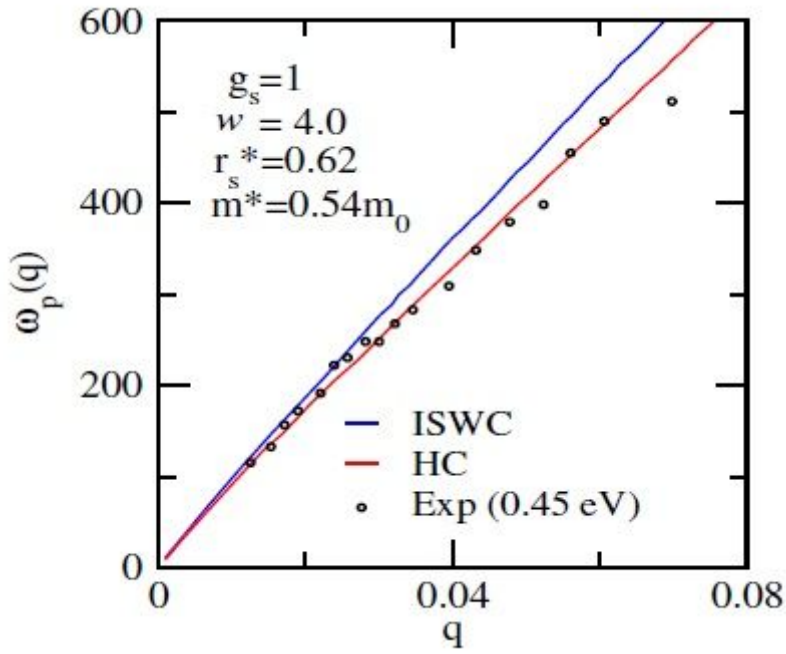
Figure 8

The variation of !p(q) (meV) vs q at indicated wire parameters in HC and ISWC models. The symbols are the experimental data of Nagao et al. [11] for electron beams having incident energy of 45eV .
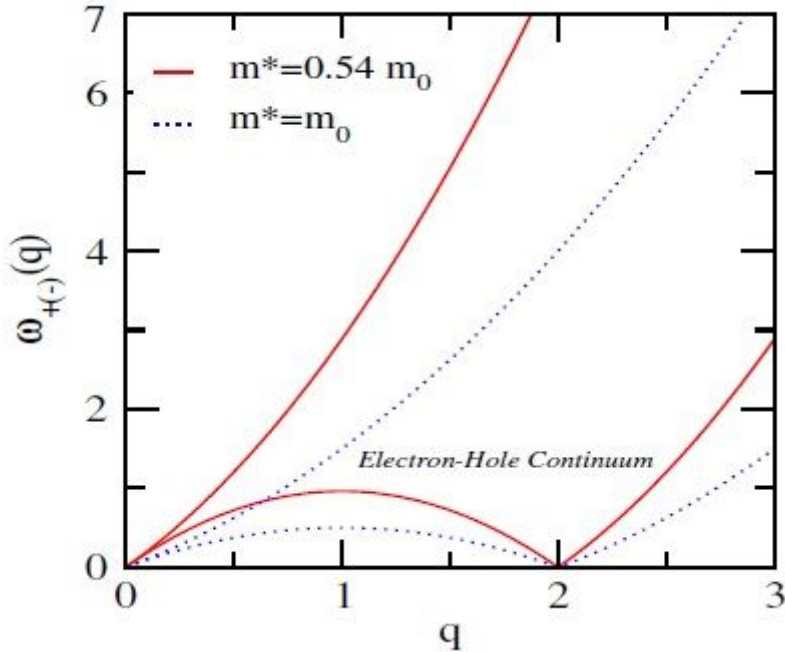
Figure 9

e-h pair continuum at m* = 0:54m0 (red solid lines) and m* = m0 (blue dotted lines).

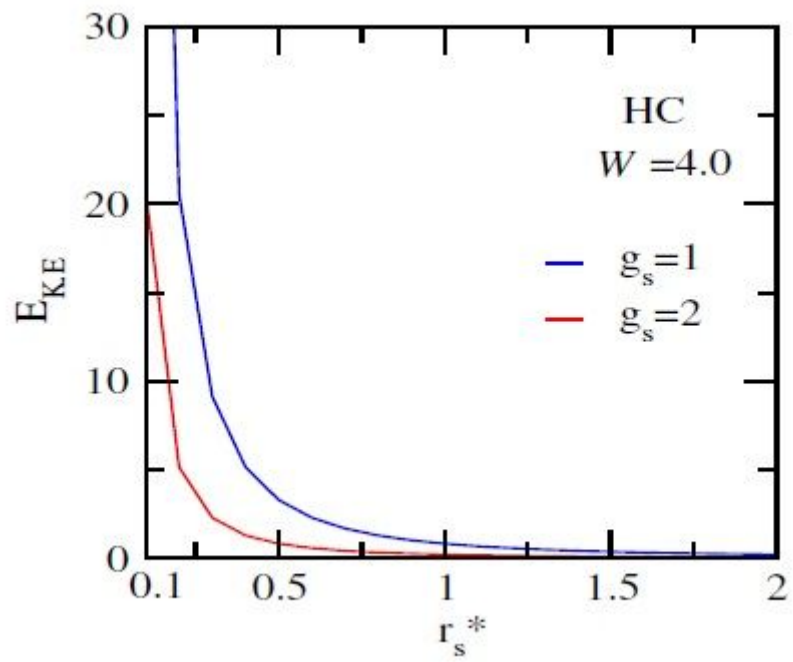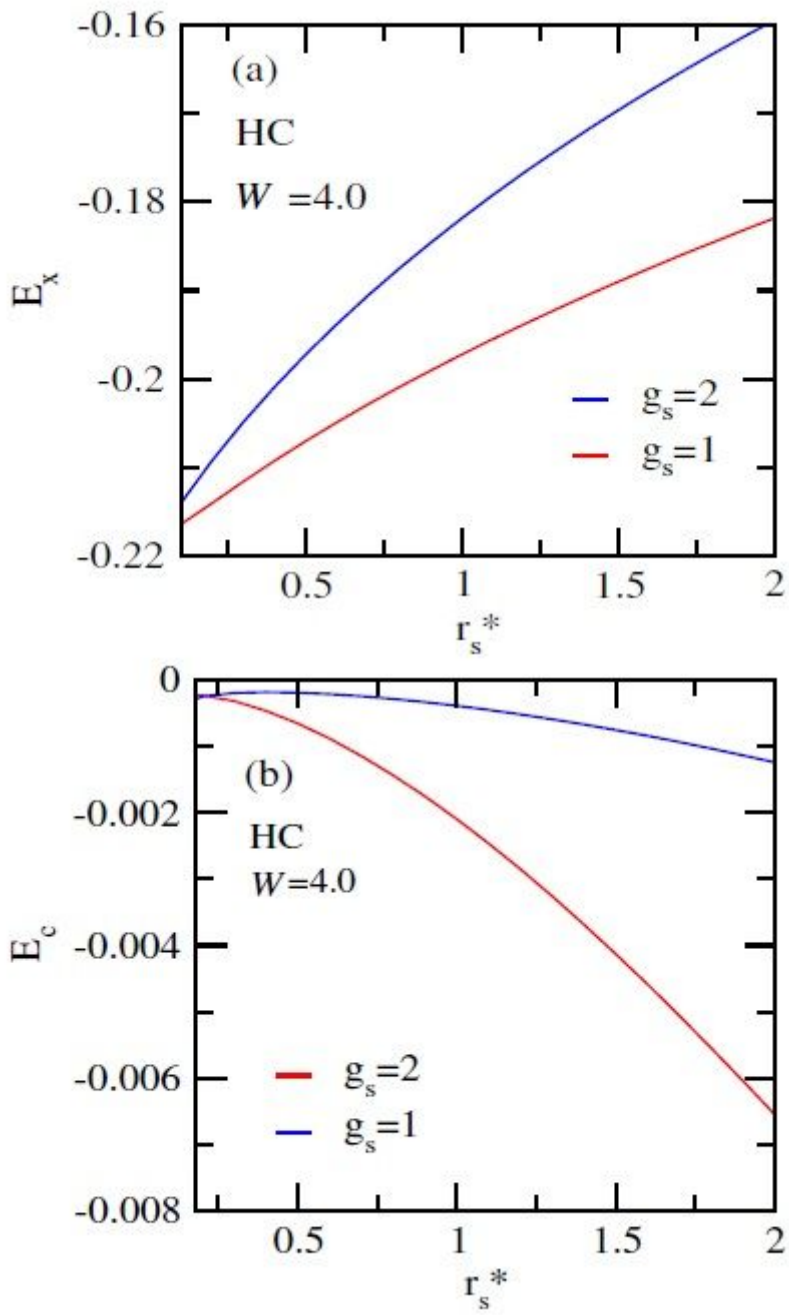**Figure 10**

The r*s -dependence of EK:E at w = 4 in HC model.

Figure 11

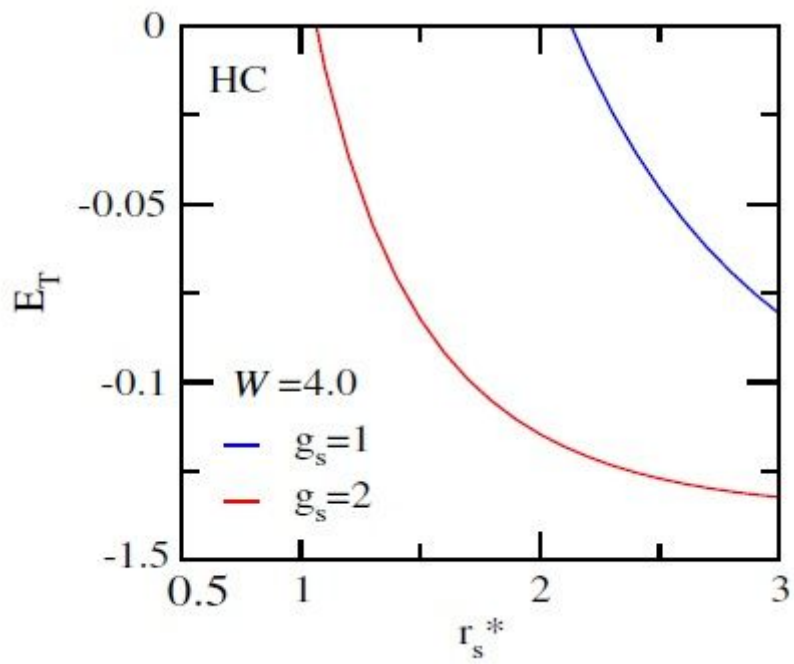The r*s -dependence of Ex [in panel (a)] and Ec [in panel (b)] at w = 4 in HC model.

Figure 12

The r*s -dependence of ET at w = 4 in HC model.